

Inhibition of ATR-Chk1 signaling blocks DNA double-strand-break repair and induces cytoplasmic vacuolization in metastatic osteosarcoma

Xiaoyang Li, Dylan C. Dean, Gregory M. Cote, Lee Zou, Francis J. Hornicek, Shengji Yu and Zhenfeng Duan 

Abstract

Background: Ataxia-telangiectasia and Rad3 related protein kinase (ATR) is an essential regulator of the DNA damage response in various cancers; however, its expression and roles in osteosarcoma are unclear. We therefore chose to evaluate the significance and mechanism of ATR in metastatic osteosarcoma, as well as its potential to be a therapeutic target.

Methods: The osteosarcoma tissue microarrays constructed from 70 patient specimens underwent immunohistochemistry to quantify ATR and activated phospho-ATR (pATR) expression and their correlation with clinical outcomes. ATR sublocalization within the metastatic osteosarcoma cells was confirmed by immunofluorescence assay. Cell proliferation, apoptosis, and migration were evaluated following treatment with ATR siRNA or the selective inhibitor Berzosertib. Antitumor effects were determined with *ex vivo* three-dimensional (3D) culture models, and the impacts on the DNA damage repair pathways were measured with Western blotting.

Results: Elevated ATR and activated pATR expression correlated with shorter patient survival and less necrosis following neoadjuvant chemotherapy. Intranuclear sublocalization of ATR and pATR suggested a mechanism related to DNA replication. ATR knockdown with siRNA or inhibition with Berzosertib suppressed cell proliferation in a time- and dose-dependent manner and induced apoptosis. In addition, ATR inhibition decreased Chk1 phosphorylation while increasing γ H₂AX expression and PARP cleavage, consistent with the interference of DNA damage repair. The ATR inhibitor Berzosertib also produced the characteristic cytoplasmic vacuolization preceding cell death, and suppressed *ex vivo* 3D spheroid formation and cell motility.

Conclusion: The faithful dependence of cells on ATR signaling for survival and progression makes it an emerging therapeutic target in metastatic osteosarcoma.

Keywords: ATR, DNA damage repair, metastatic osteosarcoma, prognostic marker, therapeutic target, tissue microarray

Received: 4 May 2020; revised manuscript accepted: 12 August 2020.

Highlights

1. ATR is overexpressed in human osteosarcoma and correlates with patient clinicopathology and prognosis.
2. ATR regulates DNA damage repair through the Chk1-dependent pathway and actively promotes osteosarcoma cell growth, proliferation, migration, and spheroid formation.
3. The suppression of ATR by its selective inhibitor Berzosertib results in characteristic cytoplasmic vacuolization and following cell death of osteosarcoma.

Ther Adv Med Oncol

2020, Vol. 12: 1–16

DOI: 10.1177/
1758835920956900

© The Author(s), 2020.
Article reuse guidelines:
sagepub.com/journals-
permissions

Correspondence to:

Shengji Yu
Department of
Orthopedics, National
Cancer Center/National
Clinical Research Center
for Cancer/Cancer
Hospital, Chinese Academy
of Medical Sciences and
Peking Union Medical
College, Beijing, 100021,
People's Republic of China
shengjiyu@126.com

Zhenfeng Duan
Sarcoma Biology
Laboratory, Department
of Orthopaedic Surgery,
David Geffen School of
Medicine at UCLA, 615
Charles E. Young Dr. S.,
Los Angeles, CA 90095,
USA
zduan@mednet.ucla.edu

Xiaoyang Li
Department of
Orthopedics, National
Cancer Center/National
Clinical Research Center
for Cancer/Cancer
Hospital, Chinese Academy
of Medical Sciences and
Peking Union Medical
College, Beijing, CHINA
Sarcoma Biology
Laboratory, Department
of Orthopaedic Surgery,
David Geffen School of
Medicine at UCLA, Los
Angeles, CA, USA

Dylan C. Dean
Sarcoma Biology
Laboratory, Department
of Orthopaedic Surgery,
David Geffen School of
Medicine at UCLA, Los
Angeles, CA, USA

Gregory M. Cote
Department of
Hematology/Oncology,
Massachusetts General
Hospital, Harvard Medical
School, Boston, MA, USA

Lee Zou
Department of
Hematology/Oncology,
Massachusetts General
Hospital, Harvard Medical
School, Boston, MA, USA
Massachusetts General
Hospital Cancer Center,
Harvard Medical School,
Charlestown, MA, USA

Francis J. Hornicek
Sarcoma Biology
Laboratory, Department
of Orthopaedic Surgery,
David Geffen School of
Medicine at UCLA, Los
Angeles, CA, USA

4. ATR is an emerging prognostic biomarker and therapeutic target in osteosarcoma.

Implication

This study identifies ATR signaling as a promising target involved in osteosarcoma-related metastatic activation.

Introduction

Osteosarcoma is the most common primary bone malignancy and causes significant mortality due to high rates of pulmonary metastasis. It has a bimodal age distribution, affecting children and adolescents as well as those in late adulthood.¹ Historically, major progress was made for osteosarcoma patients when surgical resection was combined with multiagent chemotherapy, improving the 5-year survival rate from less than 30% to nearly 70%.² However, there has since been a scarcity of emerging therapies, and outcomes for osteosarcoma patients have plateaued over the past four decades. This is especially alarming for the more than 30% of patients with localized osteosarcoma who develop recurrent or metastatic disease, as they have limited therapeutic options.³ At present, the average survival for osteosarcoma patients after recurrence or metastasis is less than a year, and there are no prognostic biomarkers within the clinic that predict chemosensitivity or metastasis.⁴ There is, therefore, a clear need for novel treatments and prognostic biomarkers in order to improve upon the limitations of older osteosarcoma therapies.

In response to DNA damage from replicative and extrinsic stress, cells activate a complex signaling network to arrest the cell cycle and repair the genome.⁵ Ataxia-telangiectasia and Rad3 related protein kinase (ATR), a serine/threonine kinase member of the ataxia-telangiectasia mutated protein kinase (ATM) subfamily, is critical in this DNA damage response (DDR).⁶ Initial recruitment of ATR to DNA damage sites activates checkpoint kinase 1 (Chk1) signaling, accelerating vital downstream pathways that prevent replicative catastrophe.^{7,8} For cancer, increased ATR expression and activation are associated with shorter patient survival as well as higher tumor grade, dedifferentiation, pleomorphism, and mitotic index.^{9,10} As cancer cells undergo unmitigated replication, they rely heavily on protective ATR signaling, and are particularly sensitive to ATR inhibition.¹¹ ATR suppression has shown

efficacy as a cancer monotherapy, and is synergistic with PARP inhibitors or radiotherapy.¹²

Because various cancers rely on a strong ATR response for DNA repair, ATR has become an attractive target in cancers, such as osteosarcoma, that have limited therapeutic options. We therefore sought to confirm the correlation of ATR with osteosarcoma patient clinicopathology and outcomes, as well as its roles in osteosarcoma cell growth, proliferation, and spheroid formation. We also explored targeted ATR therapy as a novel treatment strategy for metastatic osteosarcoma.

Material and methods

Human osteosarcoma tissue microarray and immunohistochemistry

The formalin-fixed, paraffin-embedded osteosarcoma tissue microarray (TMAs) were constructed with 70 patient specimens as previously described.^{13,14} The study was approved by the Partners Human Research Committee (#: 2007P-002464) and all patients signed a consent form for their clinical information to be used for this research. ATR and phospho-ATR (pATR) expressions were first analyzed by immunohistochemistry (IHC), with follow-up correlation with patient clinical features. The IHC-paraffin protocol was followed according to the Cell Signaling Technology company instructions. In brief, each paraffin-embedded slide was baked at 60°C for 1 h. Each section was washed in xylene for 5 min three times, then transferred through graded ethanol (100% and 95%) for 10 min twice. For antigen retrieval, endogenous peroxidase activity was quenched with 3% hydrogen peroxide. After protein blocking with normal goat serum for 1 h at room temperature, the rabbit polyclonal antibody to human ATR (1:200 dilution, #13934, Cell Signaling Technology, Beverly, MA, USA) and pATR (Ser428, 1:200 dilution, #2853, Cell Signaling Technology) was applied at 4°C overnight in a humidified chamber. The bound antibody on the array was detected by SignalStain® Boost Detection Reagent (Cell Signaling Technology) and SignalStain® DAB (Cell Signaling Technology). Prior to imaging, the section was counterstained with hematoxylin QS (Vector Laboratories, Burlingame, CA, USA) to improve nuclei imaging, and with VectaMount AQ (Vector Laboratories) for long-term preservation. Images were taken with an Olympus microscope (BX51, Olympus, Center Valley, PA, USA).

The degree of immunostaining was viewed and scored separately by two independent investigators blinded to the samples, with a joint review only done in cases of score differences.

Metastatic osteosarcoma cell lines and culture

The human metastatic osteosarcoma cell lines MNNG/HOS and 143B were purchased from ATCC (Manassas, VA, USA). Of note, both MNNG/HOS and 143B form tumors with high efficiency after injection into the proximal tibia of athymic nude mice with subsequent pulmonary metastases.^{15,16} The two cell lines tested negative for mycoplasma and bacterial contamination. They were stably cultured in RPMI-1640 (Life Technologies, Grand Island, NY, USA) supplemented with 10% fetal bovine serum (Gibco, New York, NY, USA), 100 U/ml penicillin G, and 100 µg/ml streptomycin (Life Technologies, Carlsbad, CA, USA). They were incubated in a humidified 5% CO₂ atmosphere at 37°C.

Immunofluorescence assays

Immunostaining was conducted as follows: MNNG/HOS and 143B were grown at a density of 2×10^4 cells/ml in 12-well plates for 2 days, fixed with 3.7% paraformaldehyde for 15 min, permeabilized with ice-cold methanol, then blocked with 1% bovine serum albumin (BSA). The cells were then incubated with ATR (1:100 dilution, #13934, Cell Signaling Technology) and pATR (Ser 428, 1:100 dilution, #2853, Cell Signaling Technology) primary antibodies and β -actin antibodies (1:5000 dilution, #A5316, Sigma-Aldrich, St. Louis, MO, USA) at 4°C overnight. This was followed by incubation with Alexa Fluor 488 (Green) conjugated goat anti-rabbit antibody (1:1000, #A-11034, Invitrogen, La Jolla, CA, USA) and Alexa Fluor 594 (Red) goat anti-mouse antibody (1:1000, #A-11032, Invitrogen) for 1 h. Hoechst 33342 (Life Technologies, Carlsbad, CA, USA) nuclear staining was conducted at 1:10,000 for 10 min at room temperature. Finally, the cells were imaged on a Nikon Eclipse Ti-U fluorescence microscope (Diagnostic Instruments Inc., Sterling Heights, MI, USA) equipped with a SPOT RT™ digital camera.

ATR knockdown via transfection of small interfering RNA

Transfection with ATR-specific small interfering RNA (siRNA) was performed to knockdown ATR

expression in metastatic osteosarcoma cells. The human nonspecific siRNA oligonucleotides (MISSION siRNA Universal Negative Control, # SIC001, Sigma-Aldrich) were used as a negative control. The ATR siRNA (#SASI_Hs01_00176271, 5'-GAUCCUACAUCAUGGUACA-3') was purchased from Sigma-Aldrich. Increasing concentrations (0, 10, 30, and 80 nM) of ATR siRNA and nonspecific siRNA (80 nM) were transfected into the cells using Lipofectamine® RNAiMAX Reagent (Invitrogen) according to manufacturer instructions. After 48 h for Western blot or 3, 5 or 7 days for MTT assays, the transfected cells were analyzed.

ATR inactivation with the small molecule compound Berzosertib

Berzosertib (also known as VX-970/M6620/VE-822) was purchased from Selleck (#S7102, Selleck Chemicals, Houston, TX, US). MNNG/HOS and 143B were seeded into 12-well plates at a density of 2×10^4 cells/ml and treated with increasing concentrations (0, 1.25, 2.5, 5, 10 µM) of Berzosertib for 24 h. Morphological cell changes were captured by light microscopy using a Zeiss microscope (Carl Zeiss, Inc., Oberkochen, Germany) with an attached Nikon D40 digital camera (Diagnostic Instruments Inc.) equipped with Zen Imaging software.

Cell growth and proliferation assays

For the 2-dimensional (2D) clonogenic assays, MNNG/HOS and 143B were plated into 6-well plates at 4×10^2 cells/well with different concentrations of Berzosertib upon seeding. They were cultured in growth media without antibiotics at 37°C for 7–10 days, methanol-fixed and Giemsa (GS)-stained (Sigma-Aldrich), and then underwent colony counting. These clonogenic assays were performed in triplicate.

MNNG/HOS and 143B were seeded into 96-well plates at a density of 2×10^3 cells/well and exposed to various concentrations of ATR siRNA for 5 days or Berzosertib for 3, 5, and 7 days. Treatments were performed at the time of seeding. Cell viability and cytotoxicity were assessed by MTT assays. In brief, at the end of cell treatment, 20 µl of MTT (5 mg/ml, Sigma-Aldrich) was added to each well for 4 h of incubation at 37°C. Next, the resulting formazan product was dissolved with 100 µl of acid isopropanol. The absorbance was measured at a wavelength of 490 nm (A490) on a SpectraMax Microplate®

Spectrophotometer (Molecular Devices LLC, San Jose, CA, USA). All MTT assays were performed in triplicate.

Protein preparation and western blotting

Protein lysates were extracted from MNNG/HOS and 143B with $1 \times$ radioimmunoprecipitation assay (RIPA) lysis buffer (Upstate Biotechnology, Charlottesville, VA, USA) supplemented with complete protease inhibitor cocktail tablets (Roche Applied Science, Indianapolis, IN, USA). The protein lysate concentrations were determined by DC™ protein assay reagents (Bio-Rad, Hercules, CA, USA) according to manufacturer protocol and measured with a Beckman spectrophotometer (Beckman Instruments, Inc., Indianapolis, IN, USA). Equal concentrations of denatured proteins were separated by NuPAGE® 4–12% Bis-Tris Gel (Invitrogen) then transferred to nitrocellulose membranes (Bio-Rad). After blocking with 5% non-fat milk for 1 h, the membranes were incubated with rabbit monoclonal antibodies to human ATR, pATR, phospho-Chk1 (pChk1, Ser 345, 1:1000 dilution, #2348, Cell Signaling Technology), phospho-Chk2 (pChk2, Thr 68, 1:1000 dilution, #2197, Cell Signaling Technology), phospho-ATM (pATM, Ser 1981, 1:1000 dilution, #5883, Cell Signaling Technology), phospho-histone H₂AX (γ H₂AX, Ser 139, 1:1000 dilution, #9718, Cell Signaling Technology), Bcl-xL (1:1000 dilution, #2764, Cell Signaling Technology), PARP (1:1000 dilution, #9532, Cell Signaling Technology), mouse monoclonal antibodies to human Chk1 (1:1000 dilution, #2360, Cell Signaling Technology), and β -actin at 4°C overnight. Following primary antibody incubation, the membranes were washed with TBST three times for 5 min before a Goat anti-rabbit IRDye® 800CW (#926-32211, 1:5000 dilution, Li-COR Biosciences, Lincoln, NE, USA) or Goat anti-mouse IRDye® 680LT secondary antibody (#926-68020, 1:10000 dilution, Li-COR Biosciences) was added. After incubation at room temperature for 2 h and washing with TBST an additional three times for 5 min each, the bands were detected using an Odyssey Infrared Fluorescent Western Blot Imaging System (Li-COR Bioscience). Quantifications of the Western blots were performed using Odyssey software 3.0 (Li-COR Bioscience).

Cell migration assays

Cell migration was measured by wound-healing assays. MNNG/HOS and 143B were seeded into

six-well plates at a density of 2×10^4 cells/well and incubated overnight. After they reached 100% confluency, the adherent cell layer was wounded by scraping three parallel lines with a sterile 10 μ l tip. Next, 1 μ M of Berzosertib was immediately added into the cell medium with low-serum medium containing 2% FBS, as serum starving is the most common non-pharmaceutical method for minimizing proliferation in wound healing assays.¹⁷ The wounds were observed at 0, 6, 12, 24, and 48 h after Berzosertib treatment. The wounded cells within each well were photographed at each time point with a Zeiss microscope (Carl Zeiss, Oberkochen, Germany) with a Nikon D40 digital camera (Diagnostic Instruments Inc.) and Nikon Camera Control Pro 2 Imaging software (Diagnostic Instruments Inc.). The wound width was measured as the distance between the two edges of a scratch at five sites in each image. Cell migration was determined using the following formula: percentage of wound healing (%) = [(wound width at the 0 h time point – wound width at the observed time point) / wound width at the 0 h time point] \times 100%.

Three-dimensional cell culture

Three-dimensional (3D)-cell culture can artificially simulate the *in vivo* cancer environment to better observe true growth behavior. Per the manufacturer protocol, the hydrogel 3D culture system was first prepared by diluting a hydrogel solution (VitroGel 3D-RGD, #TWG002, TheWell Bioscience, North Brunswick, NJ, USA) with deionized water in a 1:3 ratio, then mixed with complete growth media and 1 μ M of Berzosertib. Next, 50 μ l of cell suspension (2×10^4 cells/ml) was added to 200 μ l of the hydrogel 3D culture and gently transferred into a 24-well culture plate. This product was allowed to settle for 15 min for hydrogel stabilization. An additional 250 μ l of complete growth medium with 1 μ M Berzosertib treatment was then added to cover the hydrogel. The cells were incubated in a humidified 5% CO₂, 95% air atmosphere at 37°C. The media with 1 μ M Berzosertib was changed every other day to ensure adequate cell nutrition and to prevent a shift in media osmolality. After 2 weeks, light microscope images of the MNNG/HOS and 143B cell spheroids were obtained with a Zeiss microscope (Carl Zeiss) attached with a Nikon D40 digital camera (Diagnostic Instruments Inc.) and Zen Imaging software. The spheroids were also imaged on a Nikon Eclipse Ti-U

inverted fluorescence microscope (Nikon Instruments Inc., Melville, NY, USA) after 15 min of incubation with 1 μ M Calcein AM (Life Technologies). The size of cell spheroids was calculated using Image J software. The same protocol was used for controls (cell only).

Statistical analysis

Statistical analysis was performed using GraphPad PRISM 8 software (GraphPad Software, San Diego, CA, USA). Data are expressed as mean \pm SD. Student *t*-tests were used to determine the statistical significance of differences between groups. Survival analysis was assessed using the Kaplan–Meier method, and significance was determined by the log-rank test; *p* values \leq 0.05 were considered statistically significant.

Results

ATR expression is associated with osteosarcoma clinicopathology

As shown by osteosarcoma IHC staining, ATR is localized to the cytoplasm, whereas pATR resides within the nucleus. ATR staining intensity was assessed as follows: 0, no cytoplasmic staining; 1+, weak staining; 2+, moderate staining; and 3+, intense staining. These stained samples were subdivided into either a low-ATR expression group, with no (0) or a weak staining (1+); or a high-ATR expression group, with moderate (2+) or intense (3+) staining. pATR staining intensity was based on a semi-quantitative scale according to the percentage of cells with positive nuclear staining: 0, no nuclear staining; 1+, <10% positive nuclei; 2+, 10–25% positive nuclei; 3+, 26–50% positive nuclei; 4+, 51–75% positive nuclei; 5+, >75% positive nuclei. These patient specimens were then subdivided into one of the following two categories: the low-pATR expression subgroup included samples with staining <3+, and samples with a staining score \geq 3 were defined as the high-pATR expression group (Figure 1A).

ATR was expressed in most osteosarcoma patients and often in the phosphorylated state. Of the 70 patient samples, 52 (74.3%) were ATR-positive and 18 (25.7%) were ATR-negative. For the activated phosphorylation status, 53 (75.7%) were pATR-positive and 17 (24.3%) were pATR-negative (Figure 1B). No significant correlation existed between ATR or pATR expression and age, sex, or tumor. A

summary of the clinicopathological characteristics is illustrated in Table 1.

Percent tumor necrosis is a clear and accepted measurement of chemotherapeutic response. Data on percent tumor necrosis following neoadjuvant chemotherapy was available for 41 of our specimens. Of these, 6 patients showed a favorable response (\geq 90% necrosis) while the other 35 had neoadjuvant chemoresistance (<90% necrosis). Of note, those patients with chemoresistance had significantly higher expression of ATR (1.69 ± 0.14) or pATR (2.97 ± 0.25) compared with the good responders (0.33 ± 0.33 or 1.50 ± 0.62 , separately) (Figure 1C). In addition, ATR expression was significantly higher in metastatic (1.98 ± 0.18) and recurrent (2.18 ± 0.23) tissues compared with primary tumors (1.44 ± 0.12) (Figure 1F). Similar correlations were observed in pATR for metastatic (2.75 ± 0.24) and recurrent (3.00 ± 0.40) tissues compared with primary tumors (1.97 ± 0.18) (Figure 1D). All these observations were statistically significant as *p* < 0.05. We outline the relationships between ATR or pATR expression and clinical features in osteosarcoma patients in Table 2.

High ATR expression is inversely correlated with osteosarcoma patient prognosis

We next examined the association between ATR or pATR expression and osteosarcoma patient outcomes. Based on patient follow-up data up to 276 months, ATR expression was significantly higher in patients who died (non-survival; 1.70 ± 0.15) compared with those who survived (survival; 1.10 ± 0.18). In addition, pATR expression was also higher in patients who died (2.58 ± 0.20) compared with those living (1.17 ± 0.25) (Figure 1E). Spearman's rank correlation showed patient prognosis is inversely correlated with ATR expression (*r* = -0.37) and pATR expression (*r* = -0.42) (Figure 1F). Kaplan–Meier analysis revealed patients with high ATR expression have significantly shorter survival (Figure 1G) and disease-free survival (Figure 1H) compared with those with low ATR expression (based on the log-rank test). Similarly, patients with high expression of pATR had significantly shorter overall survival (Figure 1G) and disease-free survival (Figure 1H) than those with low pATR expression (based on the log-rank test). The Cox proportional hazards regression survival analysis is summarized in Table 3 (*p* < 0.05).

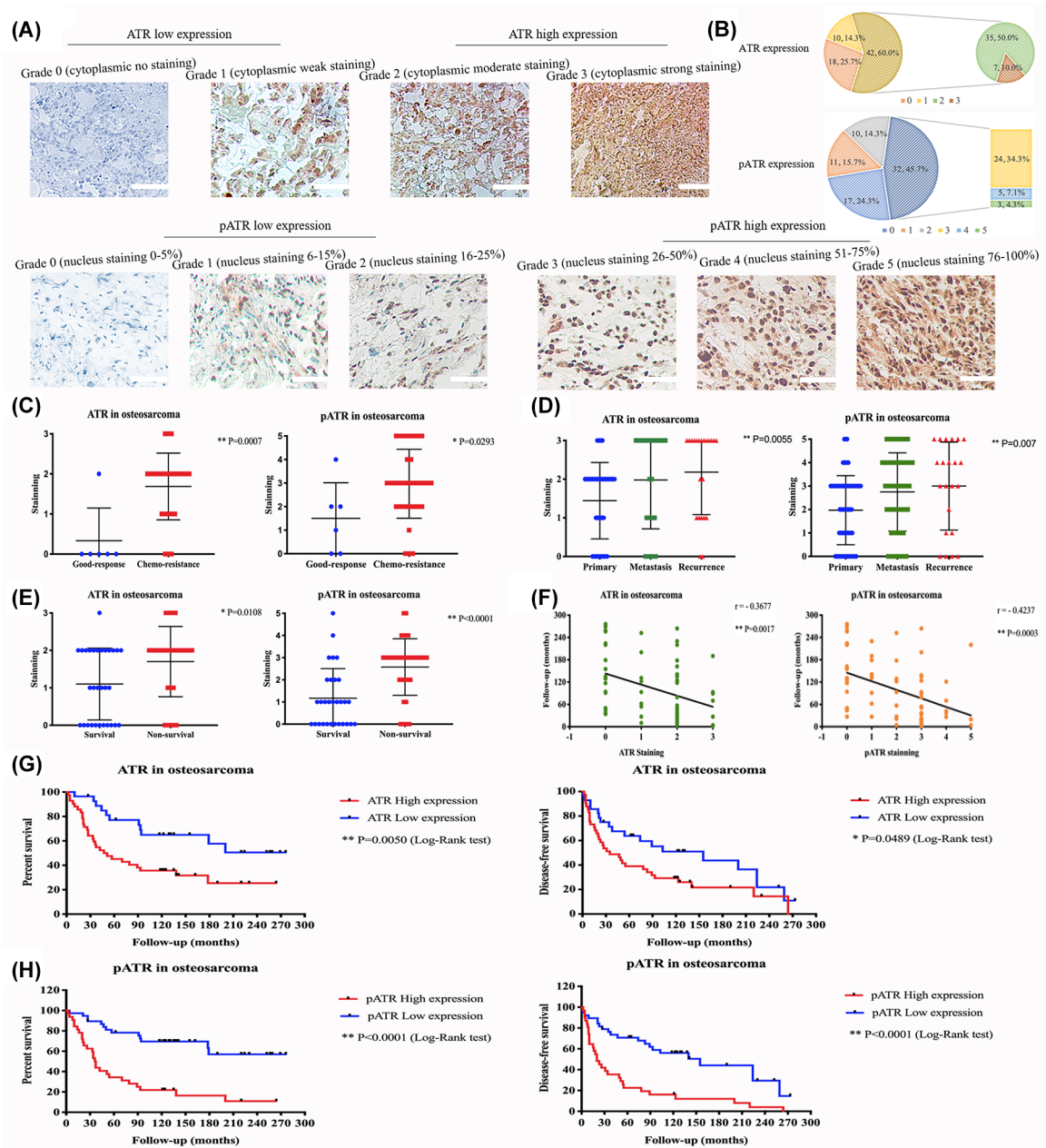


Figure 1. IHC staining of ATR in an osteosarcoma TMA correlates to chemo-response, tumor progression, and patient prognosis. ATR and activated pATR expression in a TMA constructed from 70 osteosarcoma patient samples evaluated by IHC. (A) Representative images of the TMA ATR and pATR staining (200 \times ; scale bar: 100 μ m). Four subgroups were defined according to ATR staining intensity in the cytoplasm. The stained samples were then subdivided into either the low (0 or 1+) or high (2+ or 3+) ATR expression group. Six subgroups were defined based on the percentage of cells with positive nuclear pATR staining. Again, patient samples were categorized as being in the low (staining score <3) or high (staining score \geq 3) pATR expression group. (B) Pie chart represents the relative frequencies of different ATR and pATR expression amongst the osteosarcoma TMA specimens. (C) Association of ATR and pATR expression with chemo response according to percentage of histological tumor necrosis of the osteosarcoma tissues. (D) Comparison of ATR and pATR IHC staining scores among primary, metastatic, and recurrent osteosarcoma samples. (E) Comparison between ATR and pATR IHC staining scores in osteosarcoma patients that survived (survival) and those that did not (non-survival). (F) Inverse correlation between ATR and pATR expression and osteosarcoma patient clinical follow ups (based on the Spearman's rank correlation). (G) Kaplan–Meier overall-survival curve of osteosarcoma patients sub-grouped as in the ATR or pATR low-expression group and high-expression group. (H) Kaplan–Meier disease-free survival curves of osteosarcoma patients with low and high expression of ATR or pATR. * $p < 0.05$ ** $p < 0.01$. ATR, ataxia-telangiectasia and Rad3 related protein kinase; IHC, immunohistochemistry; pATR, phospho-ATR; TMA, tissue microarray.

Table 1. Correlation between ATR or pATR expression and clinicopathology of osteosarcoma patients.

Clinicopathological characteristics	Number of cases	ATR high expression	ATR low expression	p value	pATR high expression	pATR low expression	p value
Case total	70	42	28		32	38	
Age	31.22 ± 17.30	33.38 ± 16.65	28.00 ± 18.06	0.205	32.88 ± 15.59	29.84 ± 18.71	0.469
Sex							
Male	43	27	16	0.548	23	20	0.099
Female	27	15	12		9	18	
Tumor site							
Femur	34	21	13	0.530	13	21	0.680
Tibia	14	8	6		8	6	
Humerus	7	4	3		4	3	
Radius	1	0	1		1	0	
Pelvis	6	5	1		3	3	
Spine	1	0	1		0	1	
Foot	1	0	1		0	1	
Other	6	4	2		3	3	
Follow up (months)	99.94 ± 80.04	79.00 ± 70.02	131.38 ± 84.98	0.006*	62.57 ± 64.94	137.31 ± 76.87	0.000*

* $p < 0.05$.

ATR, ataxia-telangiectasia and Rad3 related protein kinase; pATR, phospho-ATR.

ATR expression in osteosarcoma cell lines and tissues

Expression of ATR and pATR in osteosarcoma cell lines and tissues was assessed *via* western blot. ATR and pATR were overexpressed in all tested osteosarcoma cell lines compared with normal osteoblast cell lines (Figure 2A) and in five osteosarcoma tissue samples (Figure 2B). Expression and activation of ATR varied between patients, as confirmed in our tumor samples. Relative expressions of ATR and pATR were compared with β -actin in the osteosarcoma cell lines and osteosarcoma tissues (Figure 2A and B).

Immunofluorescence assays were used to test the sublocalization of ATR and pATR in the metastatic osteosarcoma cell lines MNNG/HOS (Figure 2C) and 143B (Figure 2D). As previously stated, ATR is involved in controlling the DDR, with most of its function dependent on phosphorylation and nuclearization. Our immunofluorescence confirmed the IHC findings that ATR

(green) is localized to the cytoplasm (red), while pATR (green) is largely sub-nuclear (blue) in osteosarcoma cells, with yellow representing colocalization with cytoplasmic β -actin (red).

ATR is crucial for osteosarcoma cell growth and proliferation

To analyze the function of ATR specific for osteosarcoma, we added ATR-specific siRNA to knock down ATR expression. Transfection with increasing concentrations of ATR siRNA over 5 days produced a dose-dependent decrease of cell viability in both MNNG/HOS and 143B. As expected, no significant changes were seen in the cell-only control and nonspecific siRNA transfected cell groups (Figure 3A). After ATR siRNA transfection, representative micrographs showed osteosarcoma cell morphology consistent with the toxic effects of ATR knockdown (Figure 3B). Our protein expression analyses following ATR-specific siRNA knockdown confirmed the downregulation of ATR,

Table 2. Correlation between ATR or pATR expression and clinical features of osteosarcoma patients.

Clinical features	ATR expression levels (mean ± SD)	p value	ATR expression levels (mean ± SD)	p value
Chemo-response				
Good response	0.333 ± 0.817		1.500 ± 1.517	
Chemo-resistance	1.686 ± 0.832		2.971 ± 1.465	
Good-response <i>versus</i> Chemo-resistance		0.0007*		0.0293*
Tumor progression				
Primary	1.443 ± 0.987		1.971 ± 1.474	
Metastasis	1.979 ± 1.263		2.750 ± 1.670	
Recurrence	2.182 ± 1.097		3.000 ± 1.877	
Primary <i>versus</i> Metastasis		0.0286*		0.0292*
Primary <i>versus</i> Recurrence		0.0193*		0.0267*
Prognosis				
Survival	1.100 ± 0.960		1.167 ± 1.341	
Non-survival	1.700 ± 0.939		2.575 ± 1.279	
Survival <i>versus</i> non-survival		0.0108*		0.0001*
* <i>p</i> < 0.05. ATR, ataxia-telangiectasia and Rad3 related protein kinase.				

Table 3. Survival analysis of ATR or pATR expression in osteosarcoma.

	HR	95% CI	p value
ATR^{high} <i>versus</i> ATR^{low}			
OS	2.572	1.384–4.780	0.0050*
DFS	1.748	1.009–3.027	0.0489*
pATR^{high} <i>versus</i> pATR^{low}			
OS	4.114	2.134–7.930	<0.0001*
DFS	2.987	1.661–5.371	<0.0001*
* <i>p</i> < 0.05. ATR, ataxia-telangiectasia and Rad3 related protein kinase; CI, confidence interval; HR, hazard ratio; OS, overall survival; pATR, phospho-ATR; PFS, progression-free survival.			

pATR, and pChk1, with pChk2 and pATM showing no significant changes (Figure 3C, Supplemental Figure S2A). Moreover, decreased expression of the anti-apoptotic protein Bcl-xL supported activation of pro-apoptotic pathways (Figure 3C).

Berzosertib induces cytoplasmic vacuolization and cell death in metastatic osteosarcoma

After validating the role of ATR at the mRNA level, we proceeded to assess the effects of the ATR selective inhibitor Berzosertib on metastatic osteosarcoma cells. Similar to ATR mRNA knockdown, Berzosertib led to a dose-dependent decrease in cell viability in MNNG/HOS and 143B over a 7-day observation period (Figure 4A). Signs of cytotoxicity and cytoplasmic vacuolization were assessed by microscopy at multiple time points after Berzosertib exposure. With increasing doses of Berzosertib (0, 0.625, 1.25, 2.5, 5, 10 μM) for 48 h, the osteosarcoma cells showed morphologic signs of toxicity including abnormal shape, cellular lysis, and destruction. The cells began to show observable signs of toxicity *via* cell reduction and abnormal morphology with 1.25 μM of Berzosertib. Changes were increasingly pronounced up to drug concentrations of 10 μM (Figure 4B).

More specific changes following Berzosertib treatment included cytoplasmic vacuolization, and

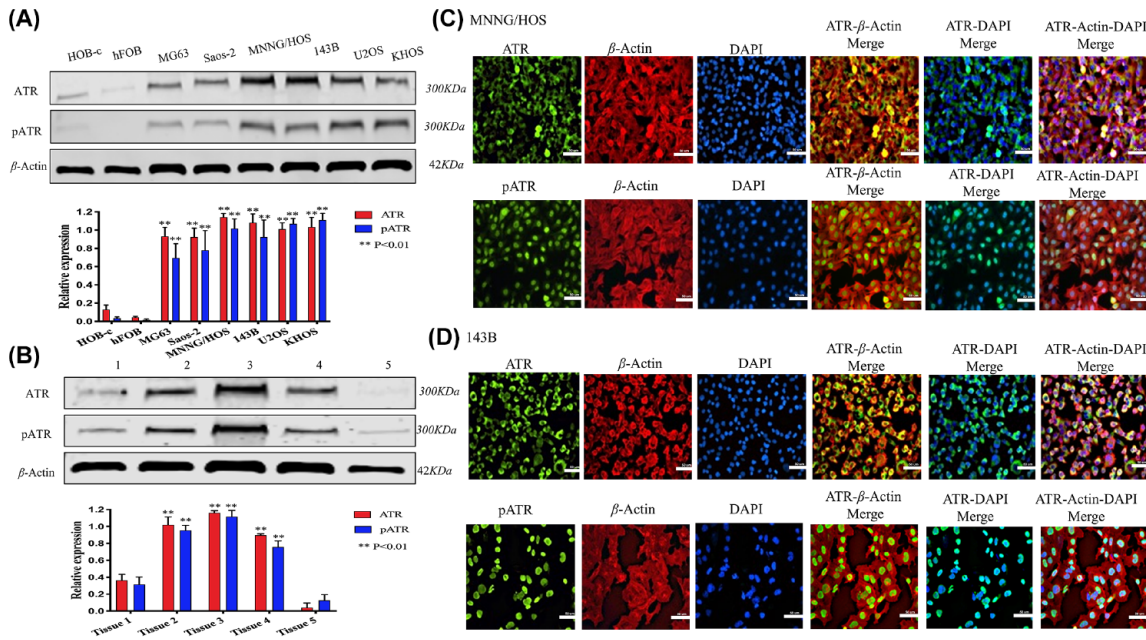


Figure 2. Expression of ATR and pATR in osteosarcoma cell lines and clinical fresh patient tissues. (A) Expression levels of ATR and pATR in osteosarcoma cell lines (MG63, Saos-2, MNNG/HOS, 143B, U2OS and KHOS) are higher than that in normal osteoblast cell lines (HOB-c and hFOB) as measured by western blot. Relative densitometry quantification of the expressions of ATR and pATR compared with β -Actin in osteosarcoma cell lines are showed below. ** $p < 0.01$. (B) ATR and pATR expressions in fresh human osteosarcoma tissues measured by western blot. Followed are the relative densitometry quantification of the expressions of ATR and pATR compared with β -actin in fresh human osteosarcoma tissues. ** $p < 0.01$. The data are mean \pm SD of the experiments carried out in triplicate. (C and D) Representative images of the localization of ATR and pATR as determined by immunofluorescence in MNNG/HOS cells (C) and 143B cells (D). Cells were visualized by fluorescence microscopy after incubation with Alexa Fluor 488 goat anti-rabbit IgG (ATR and pATR; green) or Alexa Fluor 594 goat anti-mouse IgG (β -Actin; red) or Hoechst 33342 (blue) nuclear stain. The images were merged to show the subcellular co-localization (scale bar: 50 μ m). ATR, ataxia-telangiectasia and Rad3 related protein kinase; pATR, phospho-ATR.

occurred in a dose- and time-dependent manner (Figure 4C). As early as 2h after Berzosertib administration, vacuoles appeared in the cytoplasm, with increasing prominence at 6h to 12h. Overt signs of cell death in MNNG/HOS and 143B were very evident at 24h of Berzosertib treatment as well (Supplemental Figure S1).

ATR targeting induces DNA damage via modulating the Chk1 checkpoint

Silencing of ATR with siRNA inhibits Chk1-dependent checkpoint control and DDR in a dose-dependent manner. This was evidenced by reduced expression of active pChk1 without significantly affecting Chk1, as well as by the increased expression of the sensitive DNA damage marker γ H₂AX (Figure 3C). Following Berzosertib exposure, there was significant inhibition of ATR phosphorylation and activation, as

shown by decreased pATR and pChk1. There were no significant changes in pChk2 or pATM expression (Figure 5A,B; Supplemental Figure S2B). Western blots also showed inhibition of ATR with Berzosertib suppresses phosphorylation of Chk1, causing less Chk1 mediated signaling activity as well as increased γ H₂AX and cleaved PARP expression, consistent with DDR interference (Figure 5A,B).

Abrogation of ATR activity delays motility of metastatic osteosarcoma

Given cell migration and invasion is foundational to metastasis, and our TMA showed a strong correlation between ATR expression and osteosarcoma progression, we elected to examine cell motility *via* wound-healing migration assays. In short, inhibition of ATR suppressed metastatic osteosarcoma cell motility as illustrated by our accompanying

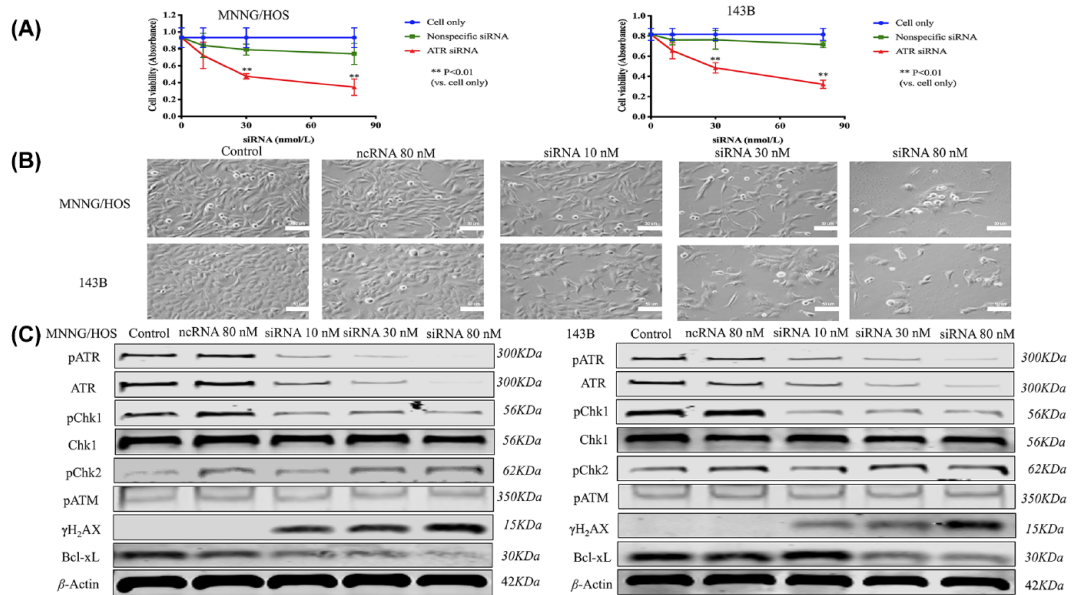


Figure 3. Knockdown of ATR with siRNA decreases cell growth through inhibition of DNA damage repair in metastatic osteosarcoma cells. (A) MTT assays demonstrate a dose-dependent reduction of cell viability after ATR siRNA transfection in MNNG/HOS and 143B cell lines. $**p < 0.01$ compared with the cell only (untreated) group. (B) Representative images of the morphologic changes in osteosarcoma cells by microscopy after ATR siRNA treatment (scale bar: 50 μm). (C) The expression of pATR, ATR, pChk1, Chk1, pChk2, pATM, $\gamma\text{H}_2\text{AX}$ and apoptotic-related protein Bcl-xL assessed by Western blot in MNNG/HOS and 143B osteosarcoma cells after 48 h of siRNA transfection. The data are mean \pm SD of the experiments carried out in triplicate. ATR, ataxia-telangiectasia and Rad3 related protein kinase; pATR, phospho-ATR; siRNA, small interfering RNA.

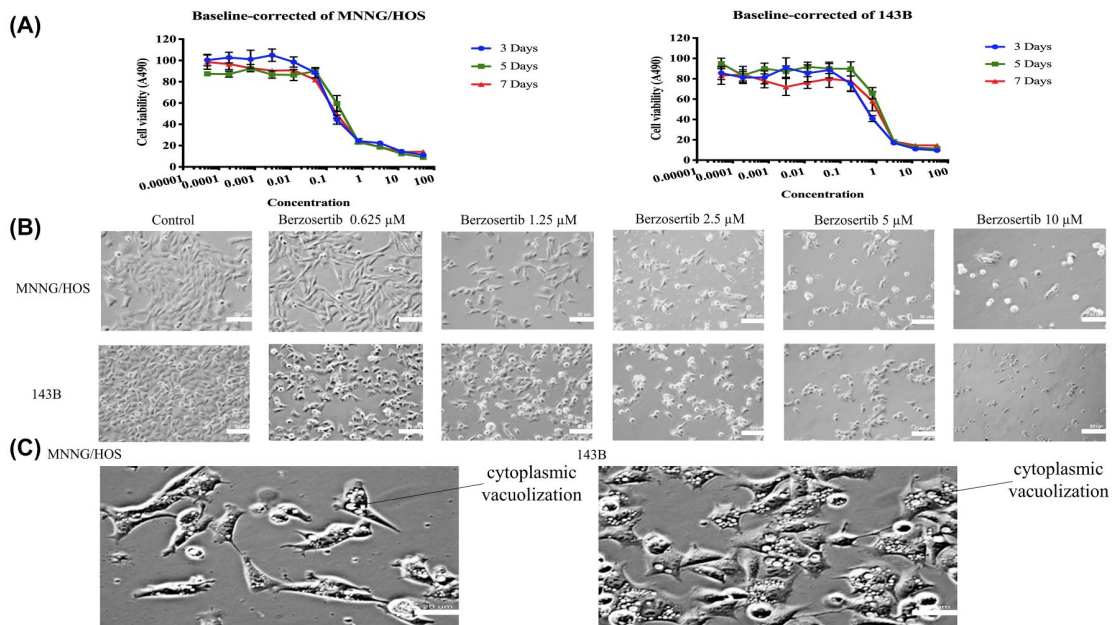


Figure 4. Inhibition of ATR activity with Berzosertib suppresses cell growth and proliferation, and induces cytoplasmic vacuolization in metastatic osteosarcoma cells. (A) Cell viability as determined by MTT assays following 48 h of Berzosertib treatment in MNNG/HOS and 143B osteosarcoma cells. The data are mean \pm SD of the experiments carried out in triplicate. (B) Representative morphologic changes in MNNG/HOS and 143B cells after increasing concentrations of Berzosertib by microscopy (scale bar: 50 μm). (C) Representative images of cytoplasmic vacuolization induced by Berzosertib in metastatic osteosarcoma cells under microscopy (scale bar: 20 μm). ATR, ataxia-telangiectasia and Rad3 related protein kinase.

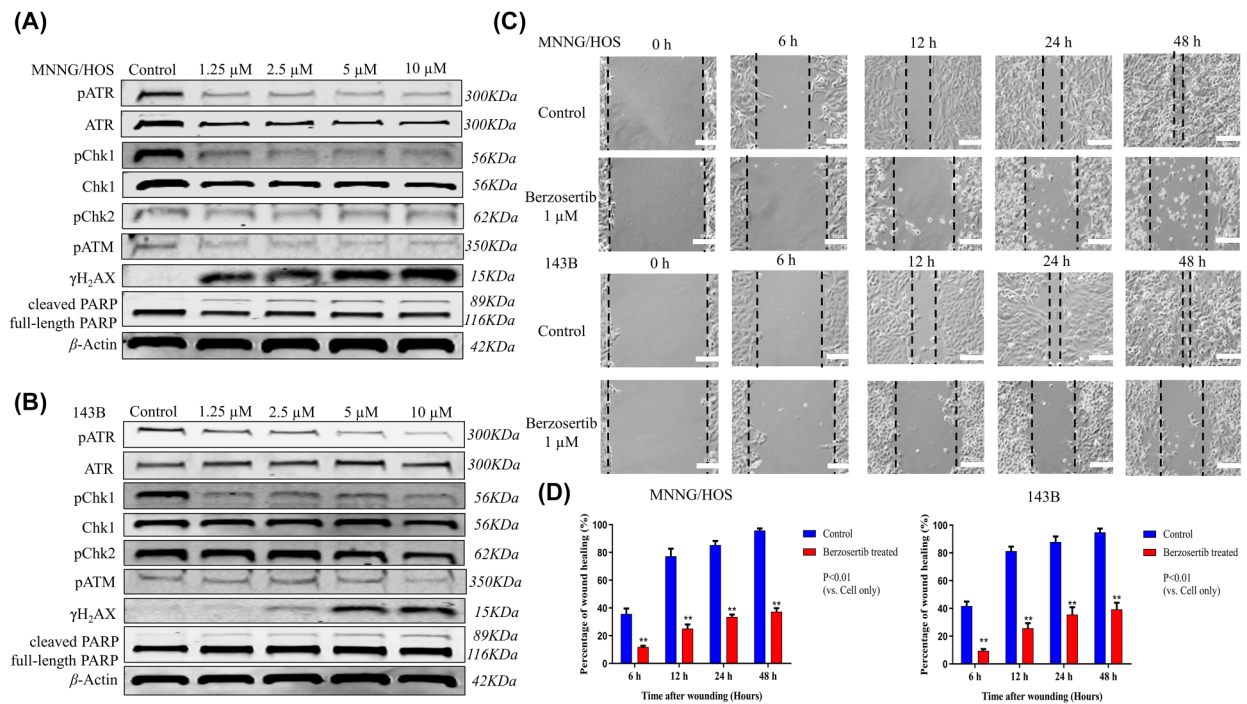


Figure 5. Treatment with Berzosertib inactivates ATR-Chk1 related pathways and reduces cell migration in metastatic osteosarcoma cells. (A, B) Western blot after 48 h of Berzosertib exposure shows decreased expression of pATR and increased expression of γ H₂AX and cleaved PARP in MNNG/HOS (A) and 143B (B) osteosarcoma cells. (C) Relative migration distance of MNNG/HOS and 143B osteosarcoma cells at different time points (0 h, 6 h, 12 h, 24 h, and 48 h) after Berzosertib treatment (scale bar: 50 μ m). (D) Cell migration distance of MNNG/HOS and 143B osteosarcoma cells after exposure to Berzosertib. ** $p < 0.01$ compared with the cell only (untreated) group. The data are mean \pm SD of experiments carried out in triplicate. ATR, ataxia-telangiectasia and Rad3 related protein kinase; pATR, phospho-ATR.

images. During the 48 h incubation period, MNNG/HOS treated with Berzosertib showed significantly decreased migration compared with the cell-only controls. Similar results were observed in the 143B metastatic cell line (Figure 5C). Relative migration distances of MNNG/HOS and 143B compared with the cell only group were charted after Berzosertib treatment at 0, 6, 12, 24, and 48 h time points (Figure 5D).

ATR inhibition reduces in vitro clonogenicity and ex vivo spheroid formation in metastatic osteosarcoma

The effect of ATR inhibition on 2D clonogenicity was evaluated *in vitro*. Berzosertib induced a dose-dependent reduction in colony formation in metastatic osteosarcoma cells (Figure 6A). 2D colony formation for MNNG/HOS and 143B compared with the untreated cell group were analyzed after 14 days of Berzosertib treatment.

Our *ex vivo* 3D cell culture model was used to mimic an *in vivo* osteosarcoma environment to

better understand how ATR inhibition affects spheroid formation in metastatic osteosarcoma. In brief, MNNG/HOS and 143B were exposed to 1 μ M Berzosertib for 14 days in 3D culture, and their resultant spheroids were photographed across 3, 5, 7, 10, and 14 days. Inhibition of ATR reduced osteosarcoma spheroid formation in the 3D culture (Figure 6B,C).

Discussion

In the present study, we show ATR and its active pATR form are highly expressed in osteosarcoma tissues and cell lines and correlate with tumor aggression. These findings are consistent with previous research demonstrating amplification and upregulation of ATR in cancers.⁹ Given percent tumor necrosis following adjuvant chemotherapy correlates with osteosarcoma chemosensitivity and prognosis,^{18,19} we analyzed these variables alongside ATR and pATR expression. We found high ATR and pATR expression to be more characteristic of chemo-resistant osteosarcomas. In addition, Kaplan–Meier survival analysis showed

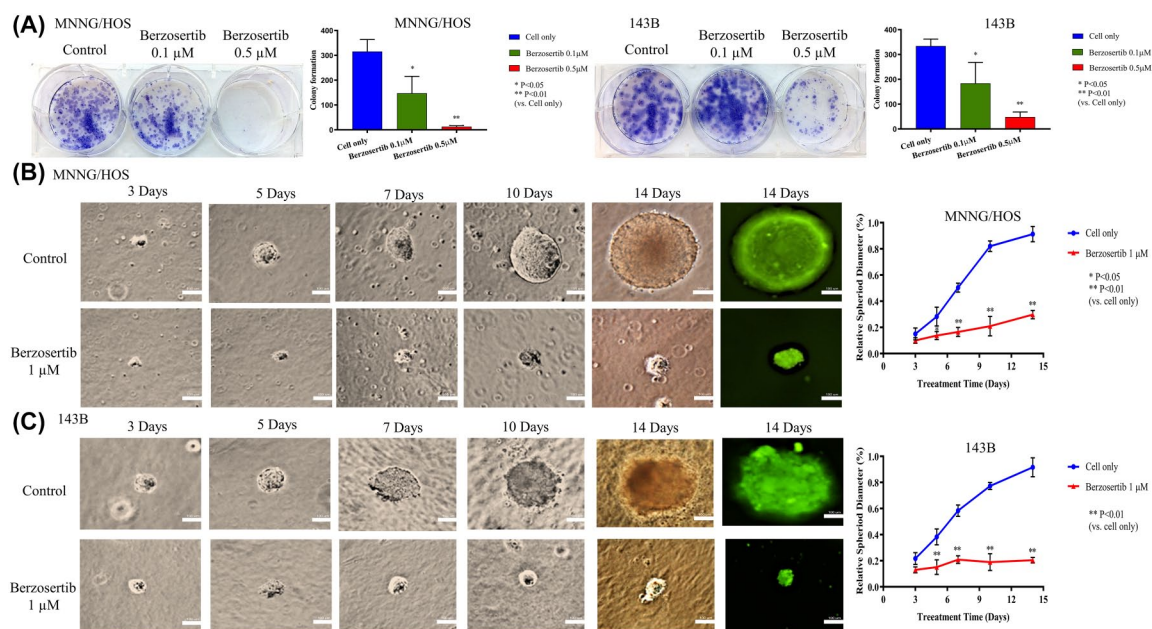


Figure 6. Inhibition of ATR with Berzosertib reduces 2D colony formation and 3D spheroid formation in metastatic osteosarcoma. (A) Representative images of cell colony formation after treatment with Berzosertib in MNNG/HOS and 143B cells. Quantification of clonogenic assays reveal a reduced rate of cell colony formation after exposure to Berzosertib in metastatic osteosarcoma cells. * $p < 0.05$, ** $p < 0.01$ compared with the cell only (untreated) group. (B and C) Representative images of MNNG/HOS (B) and 143B (C) osteosarcoma spheroids after a 14-day period in a 3D culture with or without Berzosertib treatment (scale bar: 100 μm). Relative diameters of spheroids compared with untreated groups in metastatic osteosarcoma cells. Data are mean \pm SD of the experiments carried out in triplicate. * $p < 0.05$, ** $p < 0.01$ compared with the cell only (untreated) group.

ATR, ataxia-telangiectasia and Rad3 related protein kinase; 2D, two-dimensional; 3D, three-dimensional.

elevated ATR and pATR expression correlates with poor prognosis and patient survival. These results support ATR as a prognostic biomarker in osteosarcoma.

Disruption of ATR signaling often leads to maladaptive genomic instability that is lethal to proliferating cancer.^{20,21} We show ATR is highly expressed and activated (pATR) in osteosarcoma cell lines compared with normal osteoblast cell lines, and, when inhibited, induces apoptosis. The highly selective ATR inhibitor Berzosertib has validated anticancer activity in pancreatic cancer, esophageal squamous cell carcinoma, and gastric cancer both *in vitro* and *in vivo*.^{22–25} In our study, Berzosertib increased cytoplasmic vacuolization in a dose- and time-dependent manner, and appeared alongside cell toxicity, lysis, and eventual death of the osteosarcoma cell lines. Of note, cytoplasmic vacuolization is a response characteristic of cell death.^{26–28}

Chk1 is a major downstream target of ATR which when phosphorylated facilitates cell cycle arrest

and the DDR.^{8,20,29} In osteosarcoma, we confirmed that siRNA or Berzosertib suppressed phosphorylation of Chk1 on the Ser 345 residue alongside increased γ -phosphorylation of H₂AX on the Ser 139 residue. These results show the Chk1-mediated signaling cascade helps prevent DNA double-strand breaks (DSBs) and maintains genomic integrity during replication. Additionally, ATR is a recognized core component of the DDR alongside ATM and the DNA dependent protein kinase catalytic subunits (DNA-PKcs).³⁰ Although these kinases share similar DNA sequences, they respond uniquely to DNA damage.³¹ And while the ATM/DNA-PKcs pathway is activated in response to DSBs during all cell cycle phases, ATR principally responds to DNA replication stress (RS) in a Chk1-dependent manner.^{32–34} Mechanistically, the ATR/Chk1 pathway responds to RS during cell division, where it slows replication fork elongation in order to protect against genomic instability.^{35–37} More specifically, Chk1 is activated *via* the phosphorylation of its Ser 345 residue, thus pausing replication while DNA repair takes place.^{37–39} Upon

replication fork stalling, DSBs are blocked by combined ATR-dependent fork stabilization and H₂AX/ATM/DNA-PKcs pathway activation.⁴⁰ In cancer cells, spontaneous mutation of ATM results in reliance on ATR mediated DDR; however, if ATR is also inhibited, unrepaired DNA promotes cell death.

ATR is the main kinase generating γ H2AX during replication arrest.³⁵ When ATR deficient, H₂AX rapidly undergoes γ -phosphorylation on Ser 139 (this phosphorylated form is called γ H₂AX) during the early stages of DSBs.⁴¹ Since generation of γ H2AX is abundant, fast, and correlates well with each DSB, it is a sensitive marker of DNA damage and repair.^{42–44} Because genomic instability is a hallmark of cancer, the protein kinases involved in the DDR are promising antitumor targets. Studies have shown mice with reduced expression of ATR are less tumorigenic.^{45,46} Targeting of ATR is therefore a promising avenue in osteosarcoma therapy. At present, several ATR inhibitors, including Berzosertib, are in preclinical and clinical trials.^{12,30,47} ATR plays a direct anti-apoptotic role in response to DNA damage through activating Chk1 by phosphorylation, thus halting indiscriminate mitosis entry.^{48–50}

PARP is a DNA-dependent polyadenylic acid-synthesizing nuclear enzyme involved in DNA damage repair, gene transcription, mitosis, and cell survival.⁵¹ Its activity is instrumental to the repair of DNA single-strand breaks (SSBs).^{52,53} PARP binds to SSBs and catalyzes the polymerization of ADP-ribose (PARylation), producing various polymers of ADP-ribose (PAR).⁵⁴ A loss of function of PARP weakens DNA base excision repair and accumulates SSBs and eventual DSBs through replication fork collapse, ultimately leading to cell death.⁵⁵ Our data show Berzosertib treated osteosarcoma cells have increased expression of cleaved PARP and cell apoptosis (Supplemental Figure S3). In addition, when these cells underwent knockdown of ATR with siRNA, we observed decreased antiapoptotic protein Bcl-xL, which is consistent with non-viable cancer cells.

Cell motility is crucial for the survival and dissemination of metastatic cells.⁵⁶ It is therefore a significant finding that Berzosertib reduced *in vitro* metastatic osteosarcoma cell line migration. Moreover, as 3D cell culture helps bridge *in vitro* work into a more realistic *in vivo* environment,^{57,58} we employed this platform when evaluating ATR

inhibition. Although most available *in vitro* data are based on 2D conditions, limiting cell growth to a flat plastic surface does not properly reflect multidirectional, spheroid *in vivo* growth.^{59,60} We found Berzosertib treatment delayed osteosarcoma cell spheroid growth compared with untreated cells. Collectively, these results show ATR has crucial roles in the clonogenic and spheroid osteosarcoma growth expected *in vivo*.

Conclusion

We demonstrate elevated ATR expression and activation is an independent predictor of poor prognosis in osteosarcoma patients. Inhibition of ATR induces cytoplasmic vacuolization and apoptosis through downregulation of Chk1 signaling pathways. Taken together, our study supports ATR as an emerging prognostic biomarker and promising therapeutic target in metastatic osteosarcoma.

Acknowledgements

We would like to sincerely thank the Orthopaedic Department of Massachusetts General Hospital for providing the osteosarcoma tissue samples and related clinical data. We also thank the Dana-Farber/Harvard Cancer Center for the construction of the tissue microarray.

Author contributions

X.L.: Methodology, formal analysis, data curation, writing-original draft.

D. D.: Validation, writing-editing.

G. C.: Methodology, writing-review.

Z. L.: Conceptualization, methodology.

F. H.: Investigation, resources, supervision, project administration.

S. Y.: Supervision, Funding acquisition.

Z. D.: Resources, supervision, writing-review & editing, funding acquisition.

Conflict of Interest statement

The author(s) declared no potential conflicts of interest with respect to the research, authorship, and/or publication of this article.

Funding

The author(s) disclosed receipt of the following financial support for the research, authorship, and/or publication of this article: This work was supported by the Chinese Academy of Medical

Sciences (CAMS) Innovation Fund for Medical Sciences (CIFMS) (2017-I2M-1-005), the Capital Characterized Clinical Application Research Fund of Beijing Municipal Science and Technology Commission of China (Z171100001017210), the Beijing Hope Run Special Fund of Cancer Foundation of China (LC2016L01), a Grant from Sarcoma Foundation of America (SFA) (222433) and a Grant from National Cancer Institute (NCI)/National Institutes of Health (NIH) (UO1, CA151452-01).

ORCID iD

Zhenfeng Duan  <https://orcid.org/0000-0001-7276-3910>

Supplemental material

Supplemental material for this article is available online.

References

- Moore DD and Luu HH. Osteosarcoma. In: Peabody TD and Attar S (eds) *Orthopaedic oncology: primary and metastatic tumors of the skeletal system*. Cham: Springer International Publishing, 2014, pp.65–92.
- Anderson ME. Update on survival in osteosarcoma. *Orthop Clin North Am* 2016; 47: 283–292.
- Poletajew S, Fus L and Wasiutyński A. Current concepts on pathogenesis and biology of metastatic osteosarcoma tumors. *Ortop Traumatol Rehabil* 2011; 13: 537–545.
- Maximov VV and Aqeilan RI. Genetic factors conferring metastasis in osteosarcoma. *Future Oncol* 2016; 12: 1623–1644.
- Yazinski SA and Zou L. Functions, regulation, and therapeutic implications of the ATR checkpoint pathway. *Annu Rev Genet* 2016; 50: 155–173.
- Pilié PG, Tang C, Mills GB, *et al*. State-of-the-art strategies for targeting the DNA damage response in cancer. *Nat Rev Clin Oncol* 2019; 16: 81–104.
- Qiu Z, Oleinick NL and Zhang J. ATR/CHK1 inhibitors and cancer therapy. *Radiother Oncol* 2018; 126: 450–464.
- Rundle S, Bradbury A, Drew Y, *et al*. Targeting the ATR-CHK1 axis in cancer therapy. *Cancers (Basel)* 2017; 9: 41.
- Wengner AM, Siemeister G, Lücking U, *et al*. The novel ATR inhibitor BAY 1895344 is efficacious as monotherapy and combined with DNA damage-inducing or repair-compromising therapies in preclinical cancer models. *Mol Cancer Ther*. Epub ahead of print 3 October 2019. DOI: 10.1158/1535-7163.MCT-19-0019.
- Savva C, De Souza K, Ali R, *et al*. Clinicopathological significance of ataxia telangiectasia-mutated (ATM) kinase and ataxia telangiectasia-mutated and Rad3-related (ATR) kinase in MYC overexpressed breast cancers. *Breast Cancer Res Treat* 2019; 175: 105–115.
- Flynn RL, Cox KE, Jeitany M, *et al*. Alternative lengthening of telomeres renders cancer cells hypersensitive to ATR inhibitors. *Science* 2015; 347: 273–277.
- Thomas A, Redon CE, Sciuto L, *et al*. Phase I study of ATR inhibitor M6620 in combination with topotecan in patients with advanced solid tumors. *J Clin Oncol* 2018; 36: 1594–1602.
- Gao Y, Feng Y, Shen JK, *et al*. CD44 is a direct target of miR-199a-3p and contributes to aggressive progression in osteosarcoma. *Sci Rep* 2015; 5: 11365.
- Ma H, Seebacher NA, Hornicek FJ, *et al*. Cyclin-dependent kinase 9 (CDK9) is a novel prognostic marker and therapeutic target in osteosarcoma. *EBioMedicine* 2019; 39: 182–193.
- Luu HH, Kang Q, Park JK, *et al*. An orthotopic model of human osteosarcoma growth and spontaneous pulmonary metastasis. *Clin Exp Metastasis* 2005; 22: 319–329.
- Tome Y, Tsuchiya H, Hayashi K, *et al*. In vivo gene transfer between interacting human osteosarcoma cell lines is associated with acquisition of enhanced metastatic potential. *J Cell Biochem* 2009; 108: 362–367.
- Jonkman JEN, Cathcart JA, Xu F, *et al*. An introduction to the wound healing assay using live-cell microscopy. *Cell Adh Migr* 2014; 8: 440–451.
- Man T-K, Chintagumpala M, Visvanathan J, *et al*. Expression profiles of osteosarcoma that can predict response to chemotherapy. *Cancer Res* 2005; 65: 8142–8150.
- Bacci G, Longhi A, Versari M, *et al*. Prognostic factors for osteosarcoma of the extremity treated with neoadjuvant chemotherapy: 15-year experience in 789 patients treated at a single institution. *Cancer* 2006; 106: 1154–1161.
- Weber AM and Ryan AJ. ATM and ATR as therapeutic targets in cancer. *Pharmacol Ther* 2015; 149: 124–138.
- Gorecki L, Andrs M, Rezacova M, *et al*. Discovery of ATR kinase inhibitor berzosertib

- (VX-970, M6620): clinical candidate for cancer therapy. *Pharmacol Ther* 2020; 210: 107518.
22. Lecona E and Fernandez-Capetillo O. Targeting ATR in cancer. *Nat Rev Cancer* 2018; 18: 586–595.
 23. Fokas E, Prevo R, Pollard JR, *et al.* Targeting ATR in vivo using the novel inhibitor VE-822 results in selective sensitization of pancreatic tumors to radiation. *Cell Death Dis* 2012; 3: e441.
 24. Shi Q, Shen LY, Dong B, *et al.* The identification of the ATR inhibitor VE-822 as a therapeutic strategy for enhancing cisplatin chemosensitivity in esophageal squamous cell carcinoma. *Cancer Lett* 2018; 432: 56–68.
 25. Ni F, Tang H, Wang C, *et al.* Berzosertib (VE-822) inhibits gastric cancer cell proliferation via base excision repair system. *Cancer Manag Res* 2019; 11: 8391–8405.
 26. Aki T, Nara A and Uemura K. Cytoplasmic vacuolization during exposure to drugs and other substances. *Cell Biol Toxicol* 2012; 28: 125–131.
 27. Henics T and Wheatley DN. Cytoplasmic vacuolation, adaptation and cell death: a view on new perspectives and features. *Biol Cell* 1999; 91: 485–498.
 28. Shubin AV, Demidyuk IV, Komissarov AA, *et al.* Cytoplasmic vacuolization in cell death and survival. *Oncotarget* 2016; 7: 55863–55889.
 29. Bartek J and Lukas J. Chk1 and Chk2 kinases in checkpoint control and cancer. *Cancer Cell* 2003; 3: 421–429.
 30. Jackson SP and Bartek J. The DNA-damage response in human biology and disease. *Nature* 2009; 461: 1071–1078.
 31. Falck J, Coates J and Jackson SP. Conserved modes of recruitment of ATM, ATR and DNA-PKcs to sites of DNA damage. *Nature* 2005; 434: 605–611.
 32. Smith J, Tho LM, Xu N, *et al.* The ATM-Chk2 and ATR-Chk1 pathways in DNA damage signaling and cancer. *Adv Cancer Res* 2010; 108: 73–112.
 33. Bartek J, Bartkova J and Lukas J. DNA damage signalling guards against activated oncogenes and tumour progression. *Oncogene* 2007; 26: 7773–7779.
 34. Saldivar JC, Cortez D and Cimprich KA. The essential kinase ATR: ensuring faithful duplication of a challenging genome. *Nat Rev Mol Cell Biol* 2017; 18: 622–636.
 35. Cimprich KA and Cortez D. ATR: an essential regulator of genome integrity. *Nat Rev Mol Cell Biol* 2008; 9: 616–627.
 36. López-Contreras AJ and Fernandez-Capetillo O. The ATR barrier to replication-born DNA damage. *DNA Repair (Amst)* 2010; 9: 1249–1255.
 37. Dai Y and Grant S. New insights into checkpoint kinase 1 in the DNA damage response signaling network. *Clin Cancer Res* 2010; 16: 376–383.
 38. Liu Q, Guntuku S, Cui XS, *et al.* Chk1 is an essential kinase that is regulated by Atr and required for the G(2)/M DNA damage checkpoint. *Genes Dev* 2000; 14: 1448–1459.
 39. Lin AB, McNeely SC and Beckmann RP. Achieving precision death with cell-cycle inhibitors that target DNA replication and repair. *Clin Cancer Res* 2017; 23: 3232–3240.
 40. Chanoux RA, Yin B, Urtishak KA, *et al.* ATR and H2AX cooperate in maintaining genome stability under replication stress. *J Biol Chem* 2009; 284: 5994–6003.
 41. Rogakou EP, Pilch DR, Orr AH, *et al.* DNA double-stranded breaks induce histone H2AX phosphorylation on serine 139. *J Biol Chem* 1998; 273: 5858–5868.
 42. Paull TT, Rogakou EP, Yamazaki V, *et al.* A critical role for histone H2AX in recruitment of repair factors to nuclear foci after DNA damage. *Curr Biol* 2000; 10: 886–895.
 43. Choi M, Kipps T and Kurzrock R. ATM mutations in cancer: therapeutic implications. *Mol Cancer Ther* 2016; 15: 1781–1791.
 44. Gaillard H, García-Muse T and Aguilera A. Replication stress and cancer. *Nat Rev Cancer* 2015; 15: 276–289.
 45. Murga M, Bunting S, Montaña MF, *et al.* A mouse model of ATR-seckel shows embryonic replicative stress and accelerated aging. *Nat Genet* 2009; 41: 891–898.
 46. Murga M, Campaner S, Lopez-Contreras AJ, *et al.* Exploiting oncogene-induced replicative stress for the selective killing of Myc-driven tumors. *Nat Struct Mol Biol* 2011; 18: 1331–1335.
 47. Hanahan D and Weinberg RA. Hallmarks of cancer: the next generation. *Cell* 2011; 144: 646–674.
 48. Hilton BA, Li Z, Musich PR, *et al.* ATR plays a direct antiapoptotic role at mitochondria, which is regulated by prolyl isomerase pin1. *Mol Cell* 2016; 61: 487.
 49. Brown EJ and Baltimore D. Essential and dispensable roles of ATR in cell cycle arrest and genome maintenance. *Genes Dev* 2003; 17: 615–628.

50. Thanasoula M, Escandell JM, Suwaki N, *et al.* ATM/ATR checkpoint activation downregulates CDC25C to prevent mitotic entry with uncapped telomeres. *EMBO J* 2012; 31: 3398–3410.
51. Brown JS, O’Carrigan B, Jackson SP, *et al.* Targeting DNA repair in cancer: beyond PARP inhibitors. *Cancer Discov* 2017; 7: 20–37.
52. McLornan DP, List A and Mufti GJ. Applying synthetic lethality for the selective targeting of cancer. *N Engl J Med* 2014; 371: 1725–1735.
53. Lord CJ and Ashworth A. The DNA damage response and cancer therapy. *Nature* 2012; 481: 287–294.
54. Ashworth A. A synthetic lethal therapeutic approach: poly(ADP) ribose polymerase inhibitors for the treatment of cancers deficient in DNA double-strand break repair. *J Clin Oncol* 2008; 26: 3785–3790.
55. Plummer ER and Calvert H. Targeting poly(ADP-ribose) polymerase: a two-armed strategy for cancer therapy. *Clin Cancer Res* 2007; 13: 6252–6256.
56. Friedl P and Wolf K. Tumour-cell invasion and migration: diversity and escape mechanisms. *Nat Rev Cancer* 2003; 3: 362–374.
57. Ravi M, Paramesh V, Kaviya SR, *et al.* 3D cell culture systems: advantages and applications. *J Cell Physiol* 2015; 230: 16–26.
58. van Duinen V, Trietsch SJ, Joore J, *et al.* Microfluidic 3D cell culture: from tools to tissue models. *Curr Opin Biotechnol* 2015; 35: 118–126.
59. Yamada KM and Cukierman E. Modeling tissue morphogenesis and cancer in 3D. *Cell* 2007; 130: 601–610.
60. Antoni D, Burckel H, Josset E, *et al.* Three-dimensional cell culture: a breakthrough in vivo. *Int J Mol Sci* 2015; 16: 5517–5527.

Visit SAGE journals online
journals.sagepub.com/
home/tam

 SAGE journals